A critical evaluation of decadal solar cycle imprints in the MiKlip historical ensemble simulations

Tobias C. Spiegl[1], Ulrike Langematz[1], Holger Pohlmann[2], Jürgen Kröger[2]

[1]Institute of Meteorology, Freie Universität Berlin, Berlin, Germany

[2]Max Planck Institute for Meteorology, Hamburg, Germany

Correspondence to: T. C. Spiegl (tobias.spiegl@met.fu-berlin.de)

hat gelöscht: A

Abstract

Studies concerning solar-terrestrial connections over the last decades claim to have found evidence that the quasi-decadal solar cycle can have an influence on the dynamics in the middle atmosphere in the Northern Hemisphere during winter season. It has been argued that feedbacks between the intensity of the UV part of the solar spectrum and low latitude stratospheric ozone may produce anomalies in meridional temperature gradients which have the potential to alter the zonal-mean flow in mid to high latitudes. Interactions between the zonal wind and planetary waves can lead to a downward propagation of the anomalies, produced in the middle atmosphere, down to the troposphere. More recently, it has been proposed that top-down initiated decadal solar signals might modulate surface climate and synchronize the North Atlantic Oscillation. A realistic representation of the solar cycle in climate models was suggested to significantly enhance decadal prediction skill. These conclusions have been debated controversial since then, due to the lack of missing realistic decadal prediction model set ups and more extensive analysis.

In this paper we aim for an objective and improved evaluation of possible solar imprints from the middle atmosphere to the surface and with that from head to toe. Thus, we analyze model output from historical ensemble simulations conducted with the state-of-the-art Earth system model MPI-ESM-HR. The target of these simulations was to isolate the most crucial model physics to foster basic research on decadal climate prediction and to develop an operational ensemble decadal prediction system within the MiKlip framework.

Based on correlations and multiple linear regression analysis we show that the MPI-ESM-HR simulates a realistic, statistically significant and robust shortwave heating rate and temperature response at the tropical stratopause, in good agreement with existing studies. However, the dynamical response to this initial radiative signal in the NH during the boreal winter season is weak. We find a slight strengthening of the polar vortex in midwinter during solar maximum conditions in the ensemble mean, which is consistent with the so-called "top-down" mechanism. The individual ensemble members, however, show a large spread in the dynamical response with opposite signs in response to the solar cycle, which might be a result of the large overall internal variability compensating rather small solar imprints.

We also analyze the possible surface responses to the 11-year solar cycle and review the proposed synchronization between the solar forcing and the North Atlantic Oscillation. We find that the simulated westerly wind anomalies in the lower troposphere as well as the anomalies in the mean sea level pressure are most likely independent from the timing of the solar signal in the middle atmosphere and the alleged top-down influences. The pattern rather reflects

hat gelöscht: surface solar

hat gelöscht: signals on the

hat gelöscht: might lead to a synchronization of the latter via the 11-year solar cycle

hat gelöscht: , partly

hat gelöscht: due to missing specific decadal prediction model set ups.

hat gelöscht: unbiased

hat gelöscht: which is known from

hat gelöscht: rather

hat gelöscht: In this context w

hat gelöscht: season

hat gelöscht: basically

hat gelöscht: agrees

hat gelöscht: .

hat gelöscht: seasonal march

hat gelöscht: thus

55 the decadal internal variability of the troposphere, mimicking positive and negative phases of the Arctic- and North

56 Atlantic Oscillations throughout the year sporadically, which is then assigned to the solar predictor time series without

57 any physical plausible connection and sound solar contribution.

58 Finally, by applying lead/lag correlations, we find that the proposed synchronization between the solar cycle and the

59 decadal component of the North Atlantic Oscillation might rather be a statistical artefact, affected for example by the

60 internal decadal variability of the ocean, than a plausible physical connection between the UV solar forcing and quasi-

61 decadal variations in the troposphere.

62

1. **Introduction**

The discipline of decadal climate prediction is rather young and a rapidly growing field in climate science. By using initialized climate model simulations, the gap between weather forecasting and long-term climate model projections covering the complete 21st century or beyond is bridged (e.g., Pohlmann et al., 2013; Meehl et al., 2014). By the aid of decadal climate predictions, policymakers can be equipped with an improved decision-making basis allowing for a better planning of necessary water resources, agriculture, energy and infrastructure measures for the near-term future (Mehta et al., 2011). The aim of the German joint research project "Mittelfristige Klimaprognose" (MiKlip) was to establish a new decadal prediction system allowing for a more precise midterm climate forecasting. To this effect, potential driving factors shaping the decadal climate from both anthropogenic and natural sources have been evaluated critically based on large ensemble simulations with the Max Planck Institute for Meteorology Earth System Model (MPI-ESM).

One factor that potentially influences tropospheric weather and climate is the variability in the middle atmosphere via stratosphere-troposphere coupling processes. The internal variability in the middle atmosphere during the dynamically active winter and spring seasons is strongly controlled by the variability of Rossby waves, which propagate upward from the troposphere to the middle atmosphere where they break and interact with the zonal-mean flow. The changes in the zonal-mean flow, again, can alter the propagation conditions for planetary scale waves initiating a self-consistent feedback called wave-mean flow interaction (e.g. Andrews 1985). As a result, strong disruptions, born in the middle atmosphere, such as sudden stratospheric warmings (SSWs), which are characterized by a breakdown of the polar vortex, have the potential to propagate downward into lower atmospheric layers and interfere with the tropospheric weather regime (e.g,. Baldwin and Dunkerton, 2001). A prominent example for this are Northern Hemisphere (NH) cold air outbreaks which have the tendency to be more frequent and severe in seasons with a weak stratospheric polar vortex (e.g. Huang et al., 2021).

A source of variability that might influence the dynamics in the middle atmosphere on the decadal timescale via a complex feedback mechanism between radiation, chemistry and wave-mean flow interaction is the 11-year solar cycle. Pioneering work concerning the impact of the solar cycle on middle atmosphere dynamics and possible connections to the troposphere goes back to Kodera and Kuroda (2002). Based on a relatively short period of NCEP reanalysis data (1979 – 1998), the authors observed an increase of the tropical stratopause temperature (TST) (at ~50 km) during the

98   time of the solar maximum. In their conceptual explanation, this temperature increase leads to a strengthening of the

99   meridional temperature gradient and an intensification of the polar night jet (PNJ) in the winter stratosphere. The

100 stronger westerlies create a barrier for upward propagating planetary waves, which in turn are deflected poleward and

101 break at lower altitudes. The resulting divergence in the Eliassen-Palm flux (EPF) allows the positive wind anomaly

102 to move downward and poleward over the winter season. Kodera (2002) argues that the solar induced wind anomalies

103 may advance into the troposphere, where they create a signal in meteorological variables mimicking a positive phase

104 of the North Atlantic Oscillation (NAO). Matthes et al. (2004, 2006) studied the proposed "top-down" mechanism by

105 the aid of idealized simulations with an early 3-dimensional middle atmosphere general circulation model (GCM).

106 Analysing monthly to sub-monthly means, they found that during solar maximum conditions the polar vortex seems

107 to be stronger especially in November and December and linked this to a positive Arctic oscillation (AO)-like pattern

108 which they found in lower altitudes and to some extent at the surface. The observed pattern weakens in January and

109 changes sign from February onwards. In subsequent studies comparable results have been found (e.g., Schmidt et al.,

110 2010; Ineson et al., 2011; Chiodo et al., 2012; Langematz et al., 2013). However, the exact timing of the progression

111 of the signals from the middle atmosphere to the surface depends on the individual study and varies from December

112 to February. A most recent study again concludes that the most pronounced solar signal seem to appear in early winter

113 (Ma et al. (2018)). These early studies are often quoted as convincing proof for a "top-down" influence of the 11-year

114 solar cycle in both the middle atmosphere and the troposphere. Complementary to this, Gray et al. (2013) found that

115 the strongest NAO-like solar-induced signals in the North Atlantic (i.e. a positive phase of the NAO) actually seem to

116 appear with a time lag of three to four years after the solar maximum in the respective seasonal winter mean (DJF).

117 However, the observed lags could not be reproduced in coupled atmosphere-ocean simulations conducted by the same

118 group. In the model, the postulated response to the solar cycle in the North Atlantic appears almost in phase with the

119 solar forcing (maximum response between lag year zero to one) (Gray et al., 2013). This discrepancy between observed

120 and simulated lag in the response in the North Atlantic NAO was confirmed in subsequent studies (e.g., Scaife et al.,

121 2013; Andrews et al., 2015).

122 With respect to possible solar induced impacts on NH surface variability in the winter season, Thiéblemont et al.

123 (2015) went one step further. Analyzing a simulation incorporating 150 model years, they claim that the solar forcing

124 synchronizes the decadal component of the NAO variability spectrum, a phase relation they cannot find in an

125 experiment without 11-year solar variability. This result has been debated controversially since its publication. Chiodo

hat gelöscht: convergence

hat gelöscht: penetrate

hat gelöscht: , where it is dragged towards the pole

hat gelöscht: T

hat gelöscht: Marsh et al., 2007;

hat gelöscht: , however, showing very individual temporal

hat gelöscht: s

hat gelöscht: varying

hat gelöscht: and the proposed influence in the North Atlantic region. …

hat gelöscht: ier

hat gelöscht:

hat gelöscht:

hat gelöscht:

et al. (2019) found almost identical spectra of the NAO decadal variability in two simulations of 500 model years each, with and without a 11-year solar cycle forcing. Furthermore, they identified NAO patterns in similar time segments in both experiments (forced and unforced). They suspect, therefore, that the alleged surface solar signals in other studies are most likely a result of the internal variability of the NAO itself rather than solar cycle imprints. On the other hand, Drews et al. (2022) most recently argue that the solar cycle near-surface imprints can only shine through during very active solar periods with large amplitudes of the 11-year solar cycle. They also state that during these periods the surface decadal prediction skill would be significantly enhanced if the solar cycle is a vital part of the prediction system. In the context of the most recent literature, it is difficult to understand why Chiodo et al. (2019) and Drews et al. (2022) arrive at a different assessment of the solar signal, even though the same model was used. This might point to the fact, that the complexity of the model is not the most relevant component in shaping potential surface solar signals, but rather the effects of internal variability in individual model runs and (to some degree) the applied analysis.

In this publication, we evaluate possible imprints of the 11-year solar cycle in different domains of the atmosphere from the initial solar radiative signal in the tropical upper stratosphere down to the surface in the NH winter season. We analyze the MiKlip historical ensemble simulations conducted with the state-of-the-art Earth system model MPI-ESM-HR, which is the physical basis for the decadal prediction system, which is operational at the "Deutscher Wetterdienst" (DWD) since 2020. The availability of the large amount of output data from the MiKlip historical model ensemble enables us to address the unresolved questions of the solar surface imprint, such as the dependence of the signal on the solar cycle amplitude, on a more robust statistical basis than is possible in single model simulations. In our study, we aim to identify the role of the solar imprints for the decadal variability of the NAO in winter. While the model simulations include both, changes in the total solar irradiance (TSI) and spectral solar irradiance (SSI), potential effects related to solar energetic particles (SEP) and medium energy electrons (MEE) are not explicitly included in the MiKlip experiments. Observations and model studies suggest that changes in the stratospheric composition related to SEP can lead to a radiatively driven modulation of the middle atmosphere dynamics, which can penetrate to lower atmospheric layers down to the troposphere (e.g., Seppälä et al., 2009, 2014; Baumgaertner et al., 2010; Arsenovic et al., 2016). However, since no robust surface impacts have been simulated even for strong solar energetic particle events (SEP) of the recent decades (Jackman et al., 2009), we infer that including these effects may not alter our results significantly.

167 This publication is structured as follows. In Section 2 we describe the MPI-ESM, the setup of the analyzed simulations

168 and the applied methodologies to detect potential solar cycle signals in different atmospheric domains. In Section 3,

169 the initial radiative solar signal in the tropical middle atmosphere is evaluated. Subsequently, we concentrate on the

170 dynamical response to the initial solar signal in the NH winter season. Here we show in Section 4 the ensemble mean

171 response and compare individual ensemble members with opposite solar signatures. In Section 5, we derive solar-

172 induced signals near the surface in our simulations and observations. In Section 6, we check our model results with

173 respect to the proposed synchronization between the solar forcing and the NAO. Finally, we summarize and discuss

174 our results in a broader context (Section 7).

175

176 2.   **Data and methods**

177 2.1 Model description and experimental design

178 The historical simulations analyzed in this publication have been conducted with the Max Planck Institute for

179 Meteorology Earth System Model in high resolution configuration (MPI-ESM1.2-HR; hereafter called MPI-ESM-

180 HR) at the Deutsches Klimarechenzentrum (DKRZ). MPI-ESM-HR includes the atmospheric general circulation

181 model ECHAM (European Centre Hamburg) version 6.3 (ECHAM6.3) with a horizontal/vertical resolution of

182 T127L95 (corresponds to a ~100 km * 100 km model grid and 95 levels in the vertical with a model top at 0.01 hPa

183 or ~80 km) (Müller et al., 2018). The high vertical resolution allows for an internally generated quasi-biennial

184 oscillation (QBO) in the tropical stratosphere (Pohlmann et al., 2019). Radiative processes are represented using the

185 rapid radiation transfer model for GCMs (RRTM-G) for both the shortwave and longwave part of the electromagnetic

186 spectrum (Iacono et al., 2008). Other diabatic processes, such as vertical mixing by turbulence and moist convection,

187 large-scale convection, and momentum deposition by orographic and unresolved gravity waves are described in more

188 detail in Stevens et al. (2013). Oceanic processes are accounted for in the coupled Max Planck Institute ocean model

189 (MPIOM) with a TP0.4 (0.4° nominal) resolution (Jungclaus et al., 2013). MPI-ESM-HR further incorporates the

190 biogeochemistry module Hamburg Model of the Ocean Carbon Cycle (HAMOCC) (Ilyina et al., 2013; Paulsen et al.,

191 2017) and the land surface model JSBACH (Reick et al., 2013).

192 In this publication, we analyze 10 members of the MPI-ESM-HR historical simulations performed within the German

193 research project MiKlip. The MiKlip historical ensemble simulations include the observed natural and anthropogenic

194   climate drivers, as described in the CMIP5 protocol (Taylor et al., 2013). The individual ensemble members (1 to 10)

195   have been initialized from different model years of a 1850 preindustrial (PI) control simulation and were integrated

196   over the period 1850 to 2005. Here, we focus on the period 1880 – 1999. Thus, a total of 1,200 model years have been

197   evaluated. Since the model does not include interactive atmospheric chemistry, ozone concentrations have to be

198   prescribed. In the MiKlip historical simulations, the merged CMIP5 ozone dataset was used, which consists of a

199   combination of SAGE I+II satellite and radiosonde data in the period 1979 to 2005. To derive earlier ozone

200   concentrations back to 1850, the zonal mean stratospheric time series is extended backwards based on the regression

201 fits and proxy time series of equivalent effective stratospheric chlorine (EESC) and solar variability (Cionni et al.,

202 2011). The solar variability forcing includes all observed solar cycles and follows Lean (2000).

203

204 2.1 Data analysis

205 *Detrending, correlations, filtering*

206 To detrend the sunspot number (SSN) (Source: WDC-SILSO, Royal Observatory of Belgium, Brussels -

207 https://www.sidc.be/silso/infosnmtot) and shortwave heating rate time series, a third-degree polynomial function has

208 been fitted to the data, the respective anomalies are shown in Figure 1 (the original, unfiltered SSN time series is

209 shown in Supplementary Figure 1). The detrended SSN time series has then been correlated (Pearson r) with the

210 detrended tropical stratopause temperature (defined as the mean value between 25°S – 25°N at 1 hPa (Figure 3). All

211 correlation analyses have been performed by using the Python scipy.pearsonr function. Statistical significance of the

212 correlations has been calculated by using a two-tailed Student's t-test, as implemented in Python. To reduce the

213 degree of internal variability, a Butterworth bandpass filter with cutoff frequencies of 9 and 13 years has been

214 applied to the detrended PNJ time series (defined as the arithmetic mean of the zonal-mean zonal wind between

215 35°N – 45°N at 1 hPa) (Figure 3). The same Butterworth bandpass filter has also been applied to the zonal-mean

216 zonal wind time series at 10 hPa (zonal mean over 55°N – 65°N) (Figure 3) and the NAO time series. The NAO time

217 series has been calculated by the aid of an EOF analysis conducted for the MSLP data over the Atlantic sector (20 –

218 80°N, 90°W – 40°E) in the winter season (DJF averaged and individually for December, January and February). The

219 first principal component is then used to describe the NAO variability. The lead/lag correlations (Figure 8) are then

220 calculated between the filtered NAO and SSN time series.

221 *Multiple linear regression*

222 To detect the solar cycle signals in the middle atmosphere (Figures 2, 4 and 5) and in the mean sea level pressure in

223 both observations and model data (Figures 6 and 7), we use an established multiple linear regression (MLR) technique

224 as described in Bodeker et al. (1998). To derive the individual regression coefficients, we use a set of six predictors in

225 the MLR model:

hat gelöscht: .

hat gelöscht:)

228    $X(t) = \text{Off.const} + A * CO2(t) + B * QBO(t) + C * QBOorth(t) + D * SSN(t) + E * Nino3.4(t) + F * tau(t) + R(t)$

229   with: Off.const = annual cycle; CO2(t) = increase in the atmospheric CO_2 concentration; QBO(t) = phase of the QBO,

230   defined by the zonal-mean zonal wind in 30 hPa (5°S – 5°N); QBOorth(t) = the orthogonal of QBO(t); SSN(t) = SSN

231   time series; Nino3.4(t) = Nino3.4 times series; tau(t) = optical thickness at 550 nm and R(t) = model residuum. Based

232   on this MLR analysis, we derived the model response to our chosen set of predictors, e.g., the temperature response

233   per unit of the predictor (i.e., K per 1 SSN). To display the model response during solar maximum, we scaled the

234   coefficients to 180 SSN, which is a good approximation for a mean solar cycle amplitude between 1880 and 1999. To

235   detect potential time lags in the response to the solar cycle at the surface, the solar time series has been shifted in such

236   a way that the model response lags the solar forcing by 1 to 4 years.

237

3.   The initial radiative solar signal in MPI-ESM

239   The dynamical "top-down" mechanism, assumed to be the pathway for the propagation of the solar signature through

240   the atmosphere to the surface in NH winter (see also Section 1), is initiated at the tropical upper stratosphere by the

241   absorption of solar ultraviolet (UV) irradiance by ozone and molecular oxygen. In particular, the absorption of solar

242   photons by ozone in the Hartley bands (200 – 310 nm) in the upper stratosphere - and to a lesser extent the Huggins-

243   bands (310 nm – 400 nm) in the middle stratosphere – heats the upper stratosphere increasingly with height and leads

244   to the formation of the warm stratopause. Although the variation in solar UV-irradiance over the 11-year solar cycle

245   is less than 10% in the ozone absorption bands, the enhanced UV radiation at solar maximum – in combination with

246   increased ozone concentrations - leads to stronger shortwave heating and a concurrent warming of the tropical

247   stratopause by the order of 1 K, as has been derived from merged MSU4 and SSU+MLS-satellite observations (Randel

248   et al., 2016).

249   Figure 1a shows the annual mean response of the modelled shortwave radiative heating rate (SWHR) at the

250   stratosphere and lower mesosphere (100 – 0.1 hPa) for a range of solar cycle (SC) amplitudes from the weak SC14 (in

251   blue), over the medium SC22 which has been used as solar forcing in the CMIP5 protocol (in green), to the very strong

252   SC19 (in red). MPI-EMS-HR produces the well-known solar cycle impact with enhanced SW heating during solar

253   maximum throughout the upper stratosphere and lower mesosphere. The maximum SWHR difference develops at the

hat gelöscht: The solar related coefficients have been

hat gelöscht: scaled to 1

256 stratopause and ranges for the three selected solar cycles between 0.17 and 0.51 K/day. With a SWHR increase of 0.32

257 K/day for the SC22 solar forcing, MPI-ESM-HR produces an initial solar radiative response at the tropical stratopause

258 which is in very good agreement with offline radiation model calculations using the CMIP5 solar forcing (i.e., the

259 same forcing as in MPI-ESM-HR) in a line-by-line reference and two CCM (EMAC and WACCM) radiation codes

260 (see Figure 8, yellow curves in Matthes et al., 2017). This is a significant improvement compared to the earlier

261 ECHAM4 and ECHAM5 model versions which were not able to simulate the SWHR response to the solar cycle in the

262 stratosphere (see Figure 17 in Forster et al., 2011), and thus missed the initial solar temperature signal necessary for

263 the "top-down" mechanism. The improvement in the MPI-ESM-HR is the result of the enhanced spectral resolution

264 of the new shortwave radiation scheme in ECHAM6 which resolves the shortwave spectrum in 14 bands spanning the

265 wavelength range from 820 to 50,000 cm^{-1} (Iacono et al., 2008), whereas ECHAM4 and ECHAM5 used a lower

266 spectral resolution with the four-band model of Fouquart and Bonnel (1980), later extended to six bands by Cagnazzo

267 et al. (2007).

268 Figure 1b shows the time series of the SSN and the modeled SWHR at the tropical stratopause over the period from

269 1880 – 1999. The shown anomalies of both time series from a third-degree polynomial fit clearly demonstrate that

270 solar cycles of different amplitudes initiate SWHR responses that closely follow in magnitude the strength of the solar

271 forcing. Only during SC20, the maximum SWHR response is higher than expected for that weak solar cycle. This is

272 not reproduced in the SWHR, possibly due to the transition from synthetic SSN before 1979 to observed SSN

273 afterwards.

274
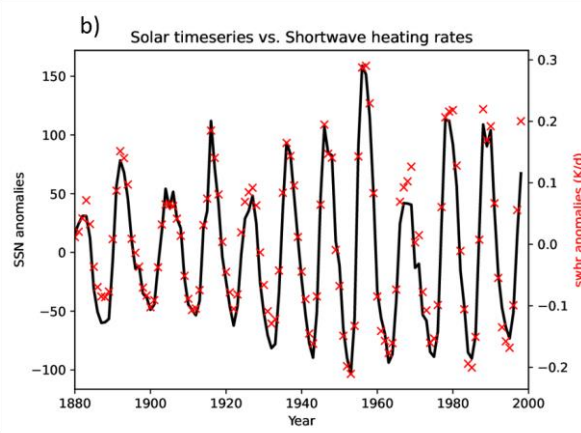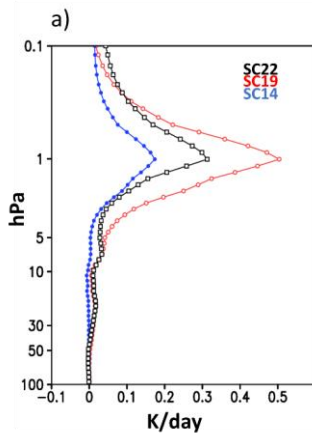
Figure 1: Solar shortwave heating rate signature in the MPI-ESM-HR historical simulations: a) Annual tropical mean (25°S – 25°N) shortwave heating rate difference in K/day between the maximum and minimum of three solar cycles: the weak solar cycle 14 (blue), the medium solar cycle 22 used in CMIP5 (green), and the strong solar cycle 19 (red) (a), and: Time series of the sunspot number and the annual tropical mean (25°S – 25°N) shortwave heating rate at the stratopause (1 hPa). Shown are anomalies from a third-degree polynomial fit to the data (b).

When averaging over all solar cycles between 1880 and 1999 and all 10 ensemble members, we obtain a robust, highly significant annual mean warming of the complete middle atmosphere at solar maximum (Figure 2a), reaching a peak response of 1.2 K at the tropical stratopause (Figure 2b). This result is slightly higher than the solar signal derived from satellite observations (0.7 K / 100 solar flux units, respectively ~1 K between solar minimum and maximum) (Randel et al., 2016). Given the excellent temporal evolution of the initial radiative response of the upper tropical stratosphere to the decadal solar forcing, we conclude that MPI-ESM-HR produces the necessary prerequisite for the dynamically enhanced "top-down"-mechanism, which will be investigated in more detail in the next section.
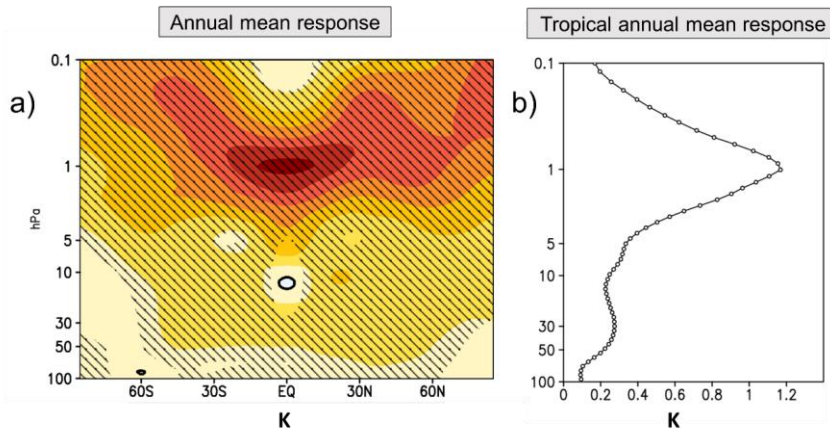
Figure 2: Long-term annual ensemble mean response based on MLR analysis of the zonal-mean temperature (in K) to the solar cycle in the middle atmosphere as a function of height and latitude (hatched regions mark the 95% level of significance) (a), and the annual mean tropical (25°S – 25°N) temperature response (in K).

4. Downward transfer of the solar signal to the surface: the key role of dynamics

After having demonstrated the ability of the MPI-ESM-HR model to realistically simulate the radiative and the related temperature response in the tropical upper stratosphere to the decadal solar forcing, we investigate as next step the

314   potential dynamical reaction to the radiative forcing, which is expected according to the "top-down" mechanism. By

315   evaluating the ensemble spread in the NH during the dynamically active season (November to March), we assess the

316   variability of different dynamical variables in the stratosphere with respect to the solar fluctuations in the MPI-ESM-

317   HR historical ensemble simulations. We focus first on the detrended deviations from the long-term monthly means for

318   the TST and (to estimate the dynamical response in the NH) the zonal-mean zonal wind at two different altitudes and

319   latitudes (Figure 3). To approximate the PNJ (the local maximum wind speed in the upper stratosphere) we use the

320   mean of the zonal-mean zonal wind in 35°– 45°N at 1 hPa. The variability in the middle stratosphere is represented

321   by the mean of the zonal-mean zonal wind in 55°– 65°N at 10 hPa. After calculating the respective anomaly time

322   series for the TST, the PNJ and the 10 hPa zonal wind variations for each month individually, we correlate these time

323   series with the detrended DJF mean SSN time series. To mute the interannual variability (operating on timescales

324   between 1 and 8 years) of the polar vortex, the PNJ and 10 hPa anomaly time series, as well as the SSN time series,

325   have been bandpass-filtered, before calculating the correlations. Our results indicate that the TST correlates

326   significantly with the SSN, not only in the annual mean (compare Figure 1b) but also in each individual month

327   considered (Figure 3, left column). While negative and positive TST anomalies (i.e. negative and positive deviations

328   from the long-term monthly mean) are almost uniformly distributed for SSN values smaller than the SC14 maximum

329   (blue dotted lines), an increase in the solar forcing exceeding the SC14 SSN maximum leads to a higher probability of

330   positive TST anomalies. The strength of the correlations changes over the season, such that a stronger connection

331   between the solar forcing and the temperature response at the tropical stratopause is given in late autumn (November:

332   r=0.28) and late winter (February: r=0.34; March: r=0.42). In these months, a particular strong solar forcing (indicated

333   by the SSN value of the SC19 maximum (red dotted lines)) is almost always associated with a positive temperature

334   anomaly at the tropical stratopause. Weaker correlations and a broader distribution of negative and positive

335   temperature anomalies, even during periods with especially pronounced solar activity, are calculated for the midwinter

336   season (December: r=0.15; January: r=0.16). These findings are consistent with an increase in the overall variability

337   in the TST during December and January, making it more difficult for the relatively weak solar induced signals to be

338   distinguished from the background noise. The higher variability in the TST during December and January is probably

339   a result of the higher variability of the tropical branch of the Brewer-Dobson circulation (BDC) in boreal winter (e.g.,

340   Butchart, 2014).

hat gelöscht:

hat gelöscht:

hat gelöscht:

hat gelöscht:

345 According to the general concept of the "top-down" mechanism the initial signal in the TST would be accompanied

346 by a strengthening of the PNJ via a modification of the meridional temperature gradients. Considering the statistically

347 significant temperature signals and correlations at the tropical stratopause in the MPI-ESM-HR model (Figure 3, left

348 column), we expect a dynamical response of the PNJ in our simulations. However, the correlations between the SSN

349 and the PNJ time series (Figure 3, middle column) do not show statistically meaningful relations between the solar

350 forcing and the dynamical response of the PNJ. Only during February, a weak but statistically significant correlation

351 is found, which might be related to the enhanced impact of the solar forcing in the TST during the same month.

352 However, this connection as well becomes insignificant, if the correlations are calculated based on the unfiltered SSN

353 and PNJ time series. Figure 3 (right column) shows the correlations between the solar forcing and the zonal mean

354 zonal wind for the lower (and more northward) 10 hPa anomaly time series. We find the strongest (and significant)

355 correlations in November ($r=0.25$) and December ($r=0.13$), although these correlations become (again) negligible if

356 the correlations are calculated based on unfiltered model data. The differences in the timing between the maximum

357 correlations of the SSN with the PNJ (February) and the 10 hPa zonal wind time series (November and December) are

358 not in line with the established idea of a successive "poleward and downward" progression of the dynamical solar

359 signal. Furthermore, the computed SSN/PNJ correlations for November, December, January and March are ≤ 0.06,

360 implying that the characteristics of the PNJ are not markedly influenced by the magnitude of the solar forcing and thus

361 the amplitude of the solar cycle.

362
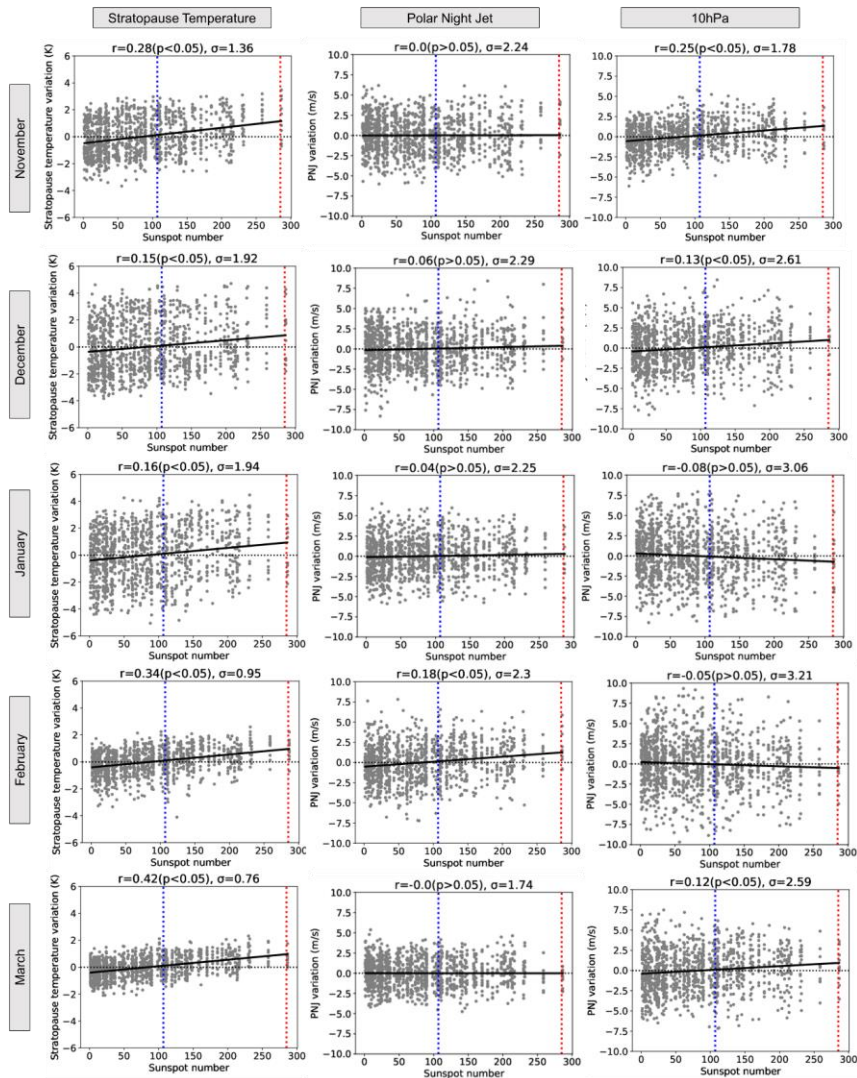
Figure 3: Scatter diagram of the stratopause temperature (left column), PNJ (middle column) and zonal-mean zonal wind averaged over 55°N – 65°N at 10 hPa (right column) variations vs. SSN. The numbers given in the headings show the correlation coefficients (r), their statistical significance (p < 0.05: significant correlation, or p > 0.05: insignificant correlation), and the overall variation (σ). The dotted blue and red lines indicate the SSN at solar cycle maximum for SC14 and SC19 (the weakest/strongest solar cycles considered in the simulations).

370   Figure 3 demonstrates that while the connection between the solar forcing and the TST is clearly visible in our

371   correlation analysis, the potential dynamical response in the NH is harder to detect, especially due to the highly variable

372   polar vortex. Therefore, we proceed using a MLR analysis to separate the potential dynamical solar induced signals

373   from other internal generated disturbances in the ensemble mean.

374   After having analyzed the variability of the TST, the PNJ and the 10 hPa zonal-mean zonal wind, we will now isolate

375   potential solar signals by the aid of MLR. Figure 4 shows the solar regression coefficients, scaled to a mean amplitude

376   of the solar cycle (180 SSN), for the zonal-mean temperature (top row), the zonal-mean zonal wind (middle row) and

377   the EPF (vectors) and its divergence EPFD (colors) (bottom row) for each NH winter month (November – March).

378   Here, we focus on the potential solar cycle signals between the equator and the North Pole and pressure heights in

379   1.000 hPa – 0.1 hPa for the temperature and wind responses and 100 hPa – 0.1 hPa for the EPF diagnostics. We find

380   a significant response in the zonal mean temperature at the tropical stratopause (Figure 4, top row) with a maximum

381   response at the equator of 1.2 K during November. The solar induced temperature signal is confined to the inner tropics

382   in late autumn and early winter and advances towards higher latitudes between January and March. This is consistent

383   with the seasonal march of the incidence angle of solar radiation after the winter solstice in December. In the middle

384   to polar latitudes, we find a clear dipole in the temperature anomalies especially during November and December.

385   This dipole is characterized by distinct (and significant) positive temperature anomalies in the lower mesosphere and

386   upper stratosphere and weak (and insignificant) negative anomalies in the middle and lower stratosphere. Particularly

387   the pronounced polar heating in the upper stratosphere from November to December agrees well with a most recent

388   analysis of ERA-interim reanalysis data by Kuroda et al., (2022). The detected temperature signals in the middle

389   atmosphere in November and December are in line with the anomalies in the zonal-mean zonal wind (Figure 4, middle

390   row), which indicate a stronger (and thus cooler) polar vortex during these months. Additionally, a convergence of the

391   EPF (indicated by the reddish colors in Figure 4, bottom row) and its (here downward oriented) vectors imply a reduced

392   upward propagation of planetary waves due to the strengthening of the polar vortex. The maximum (and significant)

393   response in the stratospheric zonal-mean zonal wind in the area of the polar vortex, is located at ~60°N at 10 hPa.

394   Here, we find positive anomalies of the zonal-mean zonal wind of ~1 m/s. Given the mean zonal-wind speeds between

395   20 m/s (November) and 30 m/s (December), simulated by the model (not shown) at this height and latitude, the solar

396   influence seems rather small in comparison. The detected dipole in the zonal-mean temperature starts to weaken from

397   January on and vanishes almost completely until March. During the same months, we find a (yet insignificant)

hat gelöscht:

hat gelöscht: ¶

hat gelöscht: analyzing

hat gelöscht:

hat gelöscht: ¶

hat gelöscht:

weakening of the polar vortex which allows for more upward propagation of planetary waves (indicated by a divergence of the EPF (bluish colors) and upward oriented vectors). In the troposphere, a weak (≤ 0.5 m/s) but significant westerly wind anomaly around ~60°N can be detected in November and December. The weak tropospheric wind response agrees with other studies (Matthes et al., 2006; Schmidt et al., 2010; Ineson et al., 2011; Chiodo et al., 2012; Langematz et al., 2013; Kuroda et al., 2022; Drews et al., 2022).

While in some studies the march of the westerly wind anomalies from the middle atmosphere to the surface seems to follow the proposed "poleward and downward" concept (e.g., Matthes et al., 2006; Ineson et al., 2011; Drews et al., 2022), the signal transmission in the MPI-ESM-HR and other model simulations (e.g., Schmidt et al., 2010; Chiodo et al., 2012; Kuroda et al., 2022) rather follows a "downward-only" storyline. Additionally, the description of the westerly wind anomalies at the surface is sometimes inconsistent with the idea of a successive downward propagation of the signal from higher to lower altitudes. As an example, significant westerly wind anomalies at the surface at middle latitudes are already present in November in the modeling studies of Matthes et al. (2006) and Kuroda et al. (2022), even though the major signal is still high up in the middle atmosphere. Furthermore, in Kuroda et al. (2022) the westerly wind anomalies at the surface at middle latitudes are present throughout the complete season (i.e., in all months between November-March), similar to our MPI-ESM-HR simulations. In other studies, the westerly anomalies are insignificant (e.g., Schmidt et al., 2010) or do not reach the ground (e.g., Chiodo et al., 2012). This implies that the detected surface wind anomalies could be independent from the seasonal march in the middle atmosphere and might rather be a product of the internal variability in the troposphere (i.e., the AO or NAO) itself. Likewise, the temperature response to the solar cycle in the troposphere with positive temperature anomalies of ≤ 0.2 K at the surface is rather weak (Figure 4, top row). Interestingly, these small temperature signals are significant in the tropics in all considered months, which is consistent with the high (and relatively constant) solar insolation in the inner tropics and a damped overall variability compared to the extratropical regions. By contrast, the significant surface temperature anomalies in the extratropical regions are located between 50°N and 60°N until January and shift towards the polar latitudes in February and March.

hat gelöscht: u

429
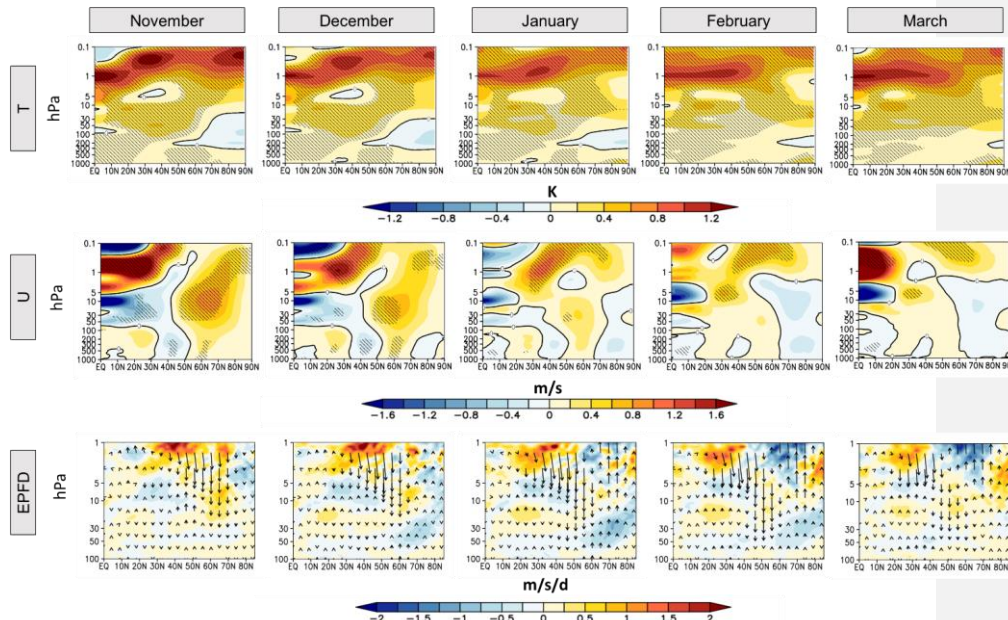
Figure 4: The ensemble mean long-term response (based on MLR) to the solar cycle of the zonal-mean temperature (first row), zonal-mean zonal wind (second row) (hatched regions mark the 95% level of significance), and the EPF (vectors) and the divergence of the EPF (EPFD, colors) in the NH during the boreal winter season. All results have been scaled to 180 SSN.

So far, we focussed on the discussion of the potential solar signals in the ensemble mean derived from the 10 individual

MiKlip historical simulations thus obtaining statistically more robust results than is possible through analyses of single

simulations. The necessity of working with ensemble mean results is impressively demonstrated by comparing two of

our 10 individual ensemble members. Figure 5 shows the solar regression coefficients for the zonal-mean temperature

and zonal-mean zonal wind for the ensemble members 1 (EM1, top panel) and 4 (EM4, bottom panel), as in Figure 4.

The derived patterns for the solar zonal-mean temperature signal in EM1 show distinct similarities with the ensemble

mean. As an example, we find a (significant) maximum temperature response around the tropical stratopause.

Furthermore, the distribution of the temperature anomalies in the middle to higher latitudes again displays the polar

heating in the lower mesosphere and the upper stratosphere and the cooling in the middle to lower stratosphere. Again,

this pattern starts to weaken from January on. We notice that in comparison to the ensemble mean, fewer areas depict

446   significant temperature signals, even though the magnitude of the temperature response is stronger. This can be

447   attributed to the fact that the analysis only includes 120 model years and thus ~12 solar cycles (instead of 1.200 and

448   ~120 in the ensemble mean), which is seemingly not enough to dampen the internal variability and inhibits the solar

449   induced signals to become significant against the overall background noise. Likewise, the solar response of the zonal-

450   mean zonal wind in the middle atmosphere in EM1 shows the main characteristics, as already noticed in the ensemble

451   mean, such as a strengthening of the polar vortex in November and December and a subsequent weakening and a

452   conversion in sign afterwards. However, none of the detected signals in the area of the polar vortex are statistically

453   significant. As for the response of the zonal-mean zonal wind at the surface, we detect significant anomalies in January

454   and February. The geographical distribution of the anomalies (westerly wind anomalies at middle latitudes and easterly

455   wind anomalies at polar latitudes), however, mimic a negative phase of the AO which is not in line with the general

456   concept of solar induced "top-down" influences.

457   In EM4, the initial temperature signal in the upper tropical stratosphere is, as in EM1, visible throughout the complete

458   season and the strongest in November and December. Thus, the response to the solar cycle in these latitudes and

459   heights turns out to be a robust feature in the MPI-ESM-HR model experiments. However, even though exactly the

460   same solar forcing has been applied in EM4 as in EM1, the dynamical response of EM4 looks very different. For

461   instance, we find a cooling of the polar upper stratosphere and a (significant) warming in the middle to lower

462   stratosphere in December and January. This pattern is common during SSWs, which (by chance) could have been

463   more frequent in EM4 during December and January than in EM1. The strong and significant easterly wind anomalies

464   in the middle atmosphere, indicating a slowdown of the polar vortex during these months, underpin this hypothesis.

465   These findings imply that the detected signals in EM1 could also be a result of (by chance) less frequent SSWs in EM1

466   leading to a potentially misleading attribution to solar variability. In our simulations, four out of 10 simulations show

467   a weakening of the polar vortex during high solar activity, while six depict a strengthening of the latter, which may

468   explain the rather weak tendency to westerly wind anomalies in the ensemble mean.

469   Either way, our results point to the fact that the internal dynamics of the polar vortex have the ability to control the

470   transmission of potential solar induced signals from the tropics to the polar regions and are thus more important than

471   the amplitudes of individual solar cycles (compare also Figure 3), as recently claimed by Drews et al. (2022).

hat gelöscht: ,

hat gelöscht: .

474

475

476
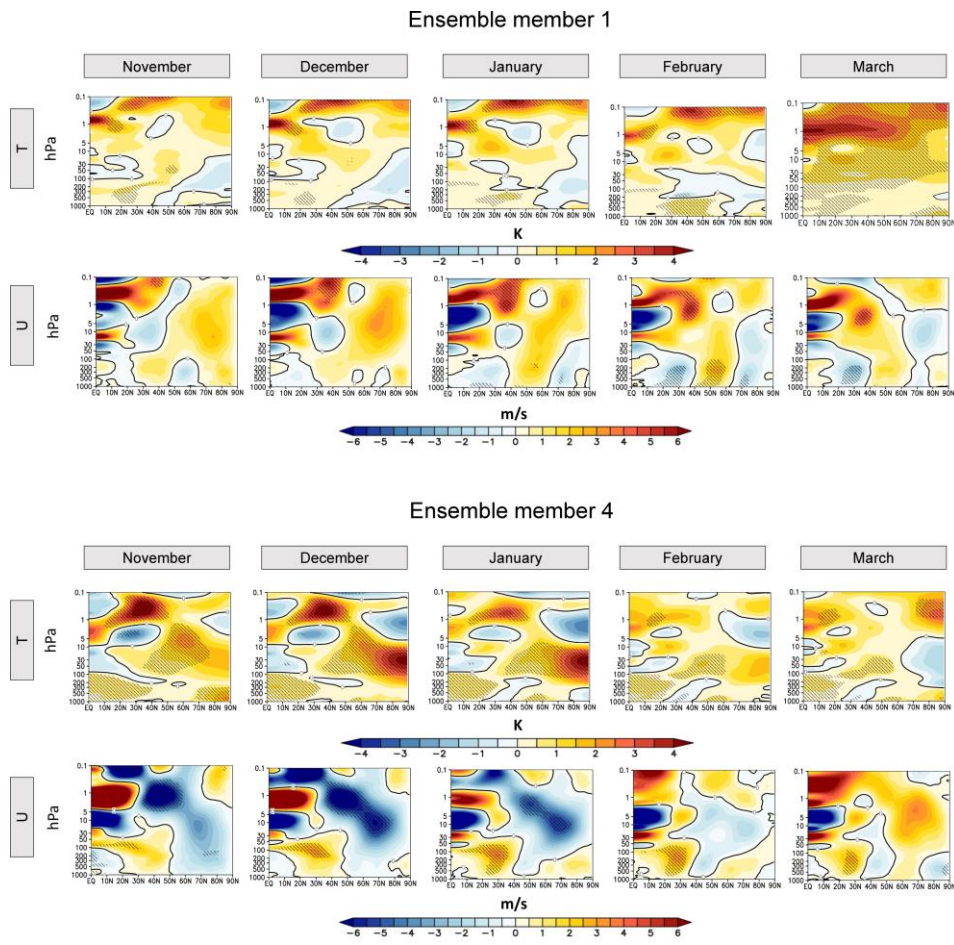
Figure 5: Long-term response (based on MLR) to the solar cycle of the zonal-mean temperature (first row) and the zonal-mean zonal wind (second row) (hatched regions mark the 95% level of significance) in the two ensemble members EM1 (top panels) and EM4 (bottom panels) in the NH during the boreal winter season. All results have been scaled to 180 SSN.

481

482

5. Direct and lagged surface solar signals

Our results so far indicate a robust response of the TST to the quasi-decadal solar cycle. The subsequent dynamical response in the NH during the boreal winter season, however, is difficult to assess. By the aid of a MLR analysis we could detect weak solar cycle imprints in the zonal-mean temperature and the zonal-mean zonal wind in the ensemble mean. However, these signals are not robust among all individual ensemble members, especially with respect to the detected anomalies in the zonal-mean zonal wind at the surface which seem to be independent of the signals in the middle atmosphere.

Nevertheless, in the next step, we first aim at detecting potential solar signals at the surface by applying the MLR analysis to mean sea level pressure (MSLP) data in NH winter. Figure 6 shows the monthly solar regression coefficients for MSLP, scaled to a mean solar cycle amplitude of 180 SSN, in the HadSLP2 observational dataset (Allan and Ansell, 2006) for the same period as simulated (1880 – 1999). In order to check for eventual time lags between the applied solar forcing and the model response, as suggested for example by Gray et al. (2013), lagged regressions were calculated by shifting the solar predictor time series against the observations so that it leads the model data between one and four years. Our results show positive and negative anomalies in the MSLP in the middle and polar latitudes which mimic positive and negative phases of the AO in a rather random than systematic way. As an example, we find an AO-positive like pattern (i.e., negative pressure anomalies over the North Pole and positive pressure anomalies in the surrounding middle latitudes) in November at lag year four, in December at lag year four, in February at the lag years one to three and in March at lag year one. The most pronounced AO-positive anomalies, with a negative but insignificant anomaly of ~2 hPa over the North Pole and a positive anomaly of the same magnitude in the middle latitudes, are given at lag year 2. Hence, the strength of the detected potential solar signals in our HadSLP2 analysis is in line with other studies assessing observational products (e.g., Gray et al., 2013; Kuroda et al., 2022; Drews et al., 2022). The detected maximum impact at lag year 2 in February in our analysis, however, agrees with Kuroda et al. (2022) and Drews et al. (2022) but differs from Gray et al. (2013) who found a maximum response at lag year 4 in the DJF mean. These discrepancies in the timing of the peak solar-induced surface signal in the HadSLP MSLP data can only be explained by differences in the analysis techniques, and reveal a high sensitivity of solar-induced surface signals to the applied methodology and individual interpretation of the results.
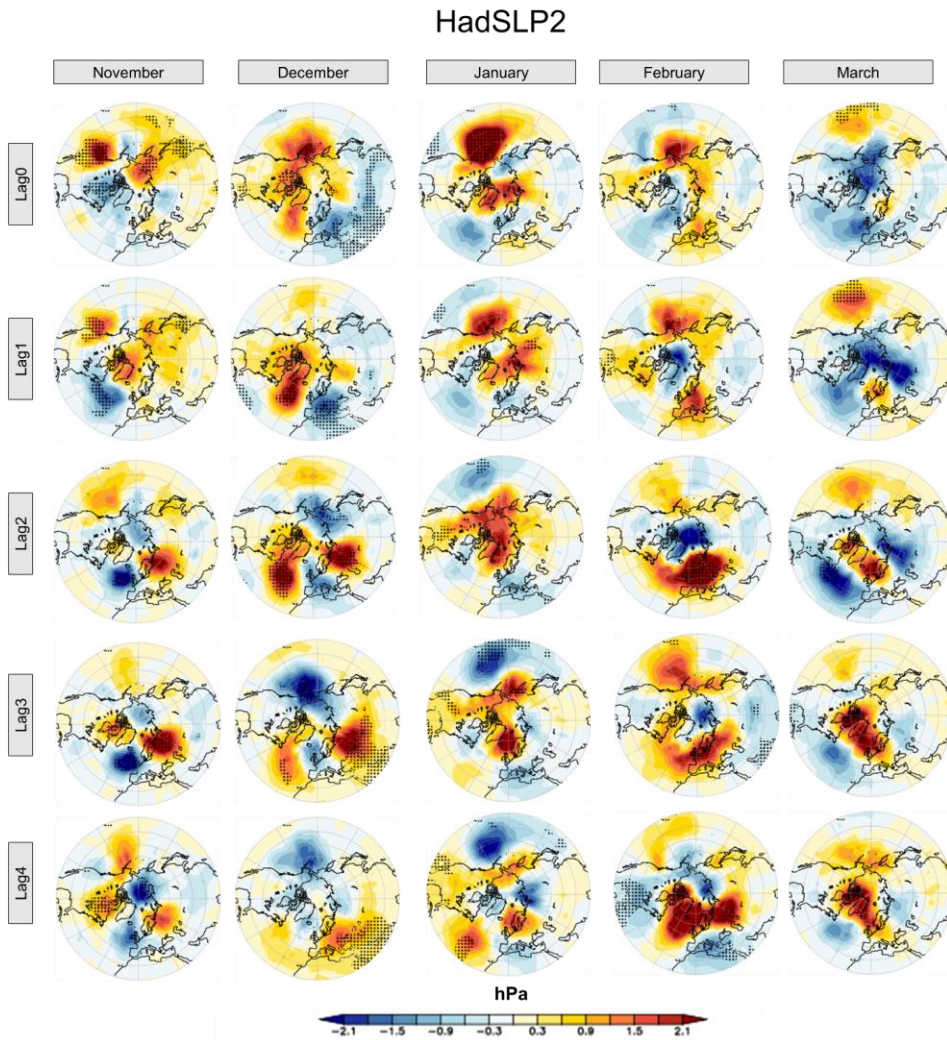
Figure 6: The (lagged) response of mean sea level pressure (MSLP) to the solar cycle in the NH during the boreal winter season for the HadSLP2 dataset (dotted regions mark the 95% level of significance). Columns denote the individual months of the winter season; rows indicate the lag of the MSLP time series with respect to the solar forcing time series.

515 Figure 7 shows the same analysis for the MiKlip historical simulations, i.e. the ensemble mean of the solar regression

516 coefficients for the MSLP for each month (November to March) and the (lag) years zero to four. We detect AO-

517 positive-like anomalies in the MSLP in December at the lag years 0 and 1, in January at the lag years 0 to 4 and in

518 February at the lag years zero to four. The strongest negative MSLP anomalies over the North Pole show a response

519 of ~ -1.5 hPa and ~ +1.5 hPa in the middle latitudes in January and December. Thus, the overall model response is

520 weaker compared to the observational data. This is not surprising given the fact that the model results depict the mean

521 over 10 ensemble members (with respective dampening effects) compared to one 'ensemble member' representing the

522 observations. While the detected magnitudes of the MSLP anomalies in MPI-ESM-HR agree with other solar cycle

523 model studies (e.g. Gray et., 2013; Scaife et al., 2013; Andrews et al., 2015; Drews et al., 2022), the detected timing

524 (i.e. the progression of the signals from the middle atmosphere to the surface) in the MPI-ESM-HR does not fit the

525 narrative of the "top-down" mechanism as described most recently by Kuroda et al. (2022) and Drews et al. (2022).

526 In these studies, the authors find the most pronounced AO-positive like pattern in February at the surface and link this

527 to the coupling between the stratosphere and the troposphere, which peaks in exactly this month. In contrast, in our

528 model simulations the strongest coupling between the stratosphere and the troposphere appears in December (see

529 Figure 4), while the most pronounced AO-positive like patterns appear in January and February at different lag years.

530 We, therefore, conclude that the detected surface solar signals could rather be a product of the internal variability in

531 the troposphere itself than being necessarily a consequence of the proposed "top-down" mechanism. Even if we assume

532 that the detected surface signals have a pure solar source (and the "top-down" mechanism is always present during

533 solar maximum years) it seems to be questionable in our view if these tiny signals would have the capability to

534 synchronize powerful large-scale climate modes such as the AO or the NAO, if they only emerge once per decade

535 over the duration of a month. As an example, the Icelandic Low and the Azores High, both controlling the pressure

536 gradients in the North Atlantic sector, show a month-by-month variation of ~8.5 hPa and ~6 hPa during winter time

537 in the model (not shown).

hat gelöscht: assume

hat gelöscht:
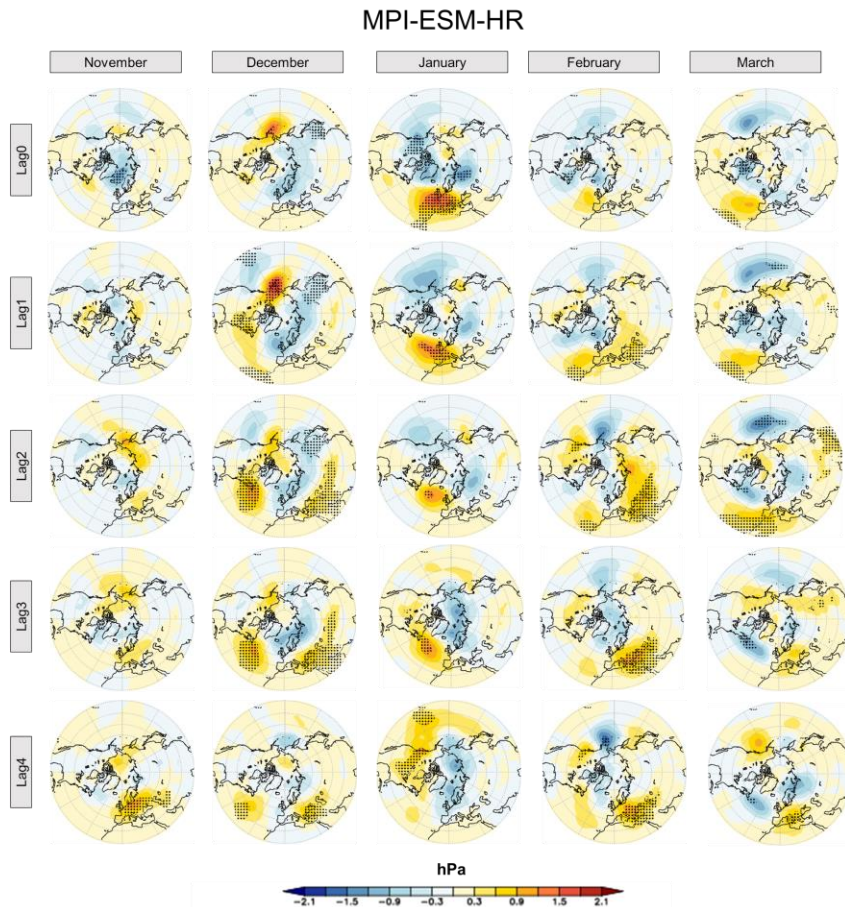
MPI-ESM-HR

540

541 **Figure 7:** As Figure 6, but for the ensemble mean of the MPI-ESM-HR MiKlip historical simulations.

542

543 **6 A synchronization of the NAO by the solar cycle?**

544 In the following, we will address the question, if the quasi-decadal variations of the solar cycle have the ability to

545 synchronize the decadal component of the NAO, as proposed by Thiéblemont et al., (2015) and Drews et al., (2022).

546 For a better comparison, we apply the same analytical strategy as proposed by Thiéblemont et al. (2015) to our model

547 simulations and the HadSLP2 data, however with the exception that we use the SSN instead of the F10.7 solar flux

times series as a solar proxy. Since both the SSN and F10.7 time series show the same oscillations on the interannual and decadal timescale, this is irrelevant for the interpretation of the results. First, an EOF analysis is applied to the deseasonalized MSLP data over the Atlantic sector (20 – 80°N, 90°W – 40°E) in the winter season (DJF averaged). The resulting leading principal components (PC1) are then used to describe the variability of the NAO. To mute major parts of the interannual variability, we apply a Butterworth bandpass filter with cutoff frequencies of 9 and 13 years to the PC1 and the SSN time series. As a result, the filtered PC1 and SSN time series only include the oscillations operating on the quasi-decadal timescale. Subsequently, lead/lag correlations are calculated between the bandpass-filtered PC1 and SSN timeseries for both the complete dataset and all individual ensemble members (1 to 10). Drews et al. (2022) recently argued that the correlations would become more meaningful during the course of the 20th century due to a series of solar cycles with stronger amplitudes. We, therefore, compute the correlations for three different time segments: the whole period (WP) (1880 – 1999), the early period (EP) with weaker solar amplitudes (1880 – 1940) and the late period (LP) with more pronounced solar amplitudes (1941 – 1999).

For the HadSLP2 dataset (Figure 8, left column/first row) positive correlations between the decadal variation of the NAO and the solar forcing is found for the lag years one to four in both the WP and the LP periods, with maximum correlations at lag year three during the LP. For the EP, we find an out-of-phase relation between the solar time series and the NAO on the decadal timescale. The evaluation of this (1 ensemble member) observational dataset implies that the solar forcing actually leads the surface response by a couple of years and that this relation is more pronounced during phases of higher solar activity. Indeed, similar phase relations in the different time segments are given in individual ensemble members of the MiKlip historical simulations (e.g., EM9 (Figure 8, left column/sixth row). However, phase relations like these seem far from being a robust feature if all model runs are considered. As an example, EM5 (Figure 8, left column/third row) indicates positive correlations between the decadal behavior of the SSN and the NAO time series for the lag years one to three during the EP, while this relation reverses (showing negative correlations) during the WP and LP. This is also true for EM3 (left column/third row) and EM7 (left column/fifth row). Other ensemble members (EM2; Figure 8, right column/second row) suggest a maximization of the solar impact at lag year zero and this independently of the considered period. Furthermore, EM6 (Figure 8, right column/fourth row) indicates stronger positive correlations at positive lag years during the EP than during the LP. The most striking discrepancies, however, come from EM1 (Figure 8, left column/second row) and EM4 (Figure 8, right column/third row). While EM1 shows negative correlations between the solar forcing and the NAO at positive lags

577   (in all time segments), this is vice versa in EM4. These surface responses in EM1 and EM4 are, however, opposite to

578   what would be expected from the polar vortex responses in these two ensemble members (a pronounced strengthening

579   of the polar vortex and a downward propagation of westerly wind anomalies to the surface in EM1, and a weakening

580   of the polar vortex and a downward propagation of easterly wind anomalies to the surface in EM4 during winter (see

581   Figure 5)) and opposite to the 'top-down mechanism'.

582   When applied to the complete dataset of the MiKlip historical simulations, the correlation analysis yields a weak

583   positive (albeit significant) correlation at the lag years two to four, rather independently of the considered time

584   segment. This, however, should rather be interpreted as a slight (and by chance) overhang to positive correlations in

585   the MiKlip dataset (that could change in a larger ensemble) than a robust physical connection between the solar forcing

586   and the NAO. To verify whether the use of the seasonal mean (DJF) might dampen the solar cycle response, as

587   discussed by Drews et al. (2022), we repeated the analysis for the individual winter months (December, January and

588   February, see Supplementary Figure 2) for the model data. We did not detect stronger connections between the decadal

589   solar forcing and the NAO in the calculations based on individual months compared to the seasonal mean. On the

590   contrary, the correlation analysis based on the December months (i.e., the month where we find the "strongest" "top-

591   down" signals in the middle atmosphere) depicts negative correlations at positive lag years. In summary, given all of

592   these inconsistencies we suspect that there is no robust connection between the quasi-decadal solar oscillations and

593   the respective phase of the NAO in the CMIP5 MiKlip historical ensemble simulations.

hat gelöscht: materia

Figure 8: Lead/lag-correlations between the seasonal mean (DJF) bandpass filtered PC1 based on NAO and SSN time series. For the HadSLP2 dataset and the ensemble mean of the MPI-ESM-HR historical simulations (top row) and the individual MPI-ESM-HR historical runs (rows 2 to 6) for different periods. Green dots mark statistically significant (95%) correlations.

7. Summary and discussion

Our analysis of the MiKlip historical ensemble simulations, conducted with the state-of-the-art Earth system model MPI-ESM-HR, revealed robust (and statistically significant) solar signals in the TST (see Figures 1 and 2). The dynamical response to the initial solar temperature signal at the tropical stratopause, in the NH middle to polar latitudes during the boreal winter season, however, showed a large spread among our data. This applies to the variability of the PNJ and the 10 hPa zonal-mean zonal wind time series, which both did not show meaningful correlations with the solar forcing (see Figure 3). When removing other than decadal variability components by MLR analysis, we were able to detect (albeit rather weak) solar signals in the NH winter, in both the ensemble mean zonal-mean temperature and zonal-mean zonal wind, that basically agree with the proposed "top-down" influence of solar variability in the middle atmosphere (see Figure 4). However, the MLR analysis based on individual ensemble members revealed signals of opposite direction (i.e., a strengthening (EM1) or weakening (EM4) of the polar vortex during periods of high solar activity) (see Figure 5). Furthermore, we find indications that the detected anomalies in the zonal-mean zonal wind at the surface are most likely independent of the signals in the middle atmosphere. The alleged surface solar signals in MSLP seem to mimic AO-positive (and AO-negative) patterns rather randomly than in a systematic way. This applies to the HadSLP2 data (Figure 6) and to the model data (Figure 7), which both depict most pronounced an AO-positive pattern in January and February at different lag years however in months, where the strong stratospheric influence (in December) is already weak or even reverses sign in the model (compare Figure 4). With respect to the suggested synchronization between the decadal solar forcing and the NAO (e.g., Thiéblemont et al., 2015) we cannot find any meaningful relations in the MiKlip historical simulations. This is supported by the fact that all ensemble members show very individual phase relations (i.e., positive/negative correlations and maximizations during different lag years) between the solar and the NAO time series. Additionally, more robust correlations could not be achieved in different time segments (i.e., periods with stronger or weaker solar forcing). These findings apply to the seasonal winter mean (DJF) as well as to individual winter months (December, January and February). As a

628 consequence, the detected phase relations in the HadSLP2 dataset should be interpreted carefully with respect to
629 potential physical connections between the solar forcing and the NAO, in particular since the observations represent
630 only one single ensemble member.

631 In summary, we draw four major conclusions:

632   1. The decadal variations of the TST in the MiKlip historical simulations are a product of the 11-year solar
633   cycle. In the course of this, an increase in the solar intensity leads to enhanced radiative shortwave heating
634   rates and a warming of the TST. These findings are consistent with other modeling studies concerning the
635   imprints of the 11-year solar cycle in the tropical upper stratosphere (Matthes et al., 2004, 2006; Schmidt et
636   al., 2010; Ineson et al., 2011; Chiodo et al., 2012; Langematz et al., 2013). The solar signals in the TST are
637   statistically significant and robust and were detected by our correlation and MLR analyses.

638   2. The dynamical response of the NH during winter in the middle atmosphere shows a weak strengthening of
639   the polar vortex during solar maximum in the ensemble mean in the MLR analysis. However, the signals
640   (especially in the zonal-mean zonal wind) are mostly insignificant and of opposite sign in individual ensemble
641   members, and thus not a robust feature. We suppose that the dynamical background state in the middle
642   atmosphere (i.e., the variability of the polar vortex) seems to play an important role for the transfer of the
643   initial radiative solar signal from the upper tropical stratosphere down to the troposphere in NH winter. The
644   important role of middle atmosphere dynamics in modulating potential solar signals is currently investigated
645   as part of the SOLCHECK project and will be published in a subsequent paper (Wenjuan Huo, personal
646   communication).

hat gelöscht: . They

hat gelöscht:

3. The detected anomalies in the zonal-mean zonal wind and MSLP at the surface seem not to be related to the timing of the seasonal march of the signals in the middle atmosphere and are most likely a manifestation of the internal variability in the troposphere itself.

4. Concerning the decadal variations of the NAO and the solar forcing, our results suggest that both are independent from each other. We find a range of phase relations between the NAO and the solar forcing throughout our ensemble members, which implies a random statistical relation rather than a physical sound connection.

It should be noted that we did not explicitly analyze a potential TSI controlled bottom-up effect on the solar surface signal, as bottom-up effects are rather confined to tropical latitudes with a prolonged influence of the TSI throughout the year (e.g., Meehl et al., 2008). Moreover, potential effects related to energetic particle precipitation are not explicitly included in the MiKlip experiments. Since these effects are known to be rather small and even less understood than the 11-year solar cycle surface imprints, we don't think they would alter our results significantly (please see the introduction section).

Since the critical study of Chiodo et al. (2019), the "top-down" mechanism and its surface imprints have been further discussed in the scientific community. It is unquestionable that early studies with GCMs and CCMs found evidence of a "top-down" mechanism in the middle atmosphere which in most cases penetrated into the troposphere in NH winter (Matthes et al., 2004, 2006; Schmidt et al., 2010; Ineson et al., 2011; Chiodo et al., 2012; Langematz et al., 2013). These studies all reproduced more or less the basic features of the "top-down" mechanism, thus confirming the physical mechanisms at work suggested by Kodera and Kodera (2002). In contrast, more recent simulations with CCMs and ESMs do not seem to find statistical responses of surface variables to the decadal solar forcing (e.g., Chiodo et al., 2019; this study). Only Drews et al. (2022) showed a near-surface solar imprint for solar cycles with strong amplitudes. The MiKlip simulations are more in line with Chiodo et al. (2019), who argued that the alleged surface solar signals could be an incidental product which is only detectable during phases with stronger solar cycles. Our results even suggest that robust solar surface imprints are basically absent throughout the complete historical period and are thus not sensitive to the amplitude of individual solar cycles. At this point we would like to emphasize that in

685 contrast to previous studies, the MiKlip simulations represent a transient climate system driven by a realistic (observed)

686 solar forcing thus enhancing the confidence in a comparison of our model results to observations.

687 We suggest that the gradual 'fading away' of significant solar near-surface signatures in more up-to-date model studies

688 is closely related to progresses made in model development and computer capacities allowing for ensemble

689 simulations. The early simulations were conducted with fixed lower boundary conditions (i.e., prescribed SSTs from

690 observations or control run experiments) (Matthes et al., 2006; Schmidt et al., 2010; Chiodo et al., 2012). Some applied

691 perpetual conditions for the solar forcing (i.e., perpetual solar maximum vs. perpetual solar minimum) and steady-

692 state conditions for the greenhouse gas forcing (Matthes et al., 2006; Schmidt et al., 2010; Ineson et al., 2011). While

693 these models included the necessary physical mechanisms, i.e., UV radiation codes and middle atmosphere dynamics,

694 to capture the solar UV-induced top-down solar signal, the complex nature of physical and chemical processes and the

695 spectrum of internal variability were reduced. Prescribed SSTs, for example, prevent the model from developing the

696 complete spectrum of interannual variability in the troposphere (e.g., induced by the internal variability of the NAO),

697 which might counteract potential surface solar signals. In addition, steady-state background conditions in atmospheric

698 greenhouse gas concentrations and prescribed ozone depleting substances do not take into account transient adjustment

699 processes in the atmospheric dynamics, which again lead to a reduction of the overall internal variability and maybe

700 an overestimation of solar-induced signals. Moreover, due to more limited computer capacities, the results from the

701 early model studies were mostly based on single simulations.

702 In contrast, our results show that in a state-of-the-art climate model system the potential solar near-surface signals are

703 rather weak, not robust and inconsistent with the timing in the middle atmosphere. One potential reason is the

704 additional variability component introduced into the model by the interactively coupled ocean model. Misios and

705 Schmidt (2012) also showed the impact of an interactive ocean on the simulated solar response in the tropical Pacific

706 region. While individual ensemble simulations produce the expected phase correlation between the NAO and the solar

707 cycle, others show the opposite behavior. Thus, we do not find any convincing evidence in our model simulations of

708 the alleged decadal synchronization between the NAO and the solar forcing, as suggested by Thiéblemont et al. (2015).

709 In our view, the decadal near-surface signals detected in the MiKlip historical simulations are a product of the internal

710 variability in the troposphere itself and not a physical consequence of the "top-down" mechanism.

711 We would further like to mention that a strong reduction of the interannual variability in two basically independent

712 time series – be it by bandpass filtering like in our study or in Thiéblemont et al. (2015), or by using wide running

hat gelöscht: Marsh et al., 2007;

hat gelöscht: Marsh et al., 2007;

hat gelöscht: disposed

hat gelöscht: of

hat gelöscht: In both cases,

hat gelöscht: is damped

hat gelöscht: mean

hat gelöscht: We, thus,

721 mean windows like in Drews et al. (2022) – will always lead to significant alignments of these two time series at some

722 point, if they are shifted towards each other gradually. Thus, the phase relations in our (and other studies) seem to be

723 a statistical artifact and not the consequence of a physical phase coupling. We also would like to question if the oceanic

724 memory is sensitive enough to store the tiny surface solar signals (even if there are some) for the duration of a complete

725 decade. Hence, in our opinion a much more profound solar forcing would be needed to significantly influence the

726 ocean temperature and thus dynamically driven feedbacks. Such forcings, however, typically operate on the centennial

727 timescale which is characterized by phases of Grands Solar Maxima and Minima (e.g., Spiegl and Langematz (2020)).

728 Also, please keep in mind the strong variability of the main pressure systems in the North Atlantic, which might wipe

729 out potential surface solar signals within a couple of months. The discrepancies between the observed and modelled

730 internal variability in response to external forcings (such as solar variability) may also be attributed to the "signal-to-

731 noise" paradox which states that relatively small changes in the external forcing will not lead to detectable changes in

732 the variability spectrum in both the real climate system and model simulations as discussed by Scaife and Smith (2018).

733 Furthermore, and in our opinion, a physically sound explanation for the alleged NAO-solar cycle phase coupling is

734 missing so far. Thus, the claim that an inclusion of the 11-year solar cycle would lead to a better understanding of the

735 decadal oscillations in the NH troposphere during winter, is not supported by our analyses of the MiKlip historical

hat gelöscht: I

737 ensemble simulations. Future studies with a distinct focus on the decadal prediction skill might help to confirm our

738 results.

739

Data availability

741 The main numerical results will be made available upon request by the authors.

Author contributions

743 TS was in charge in conducting the analysis and writing the manuscript. UL initiated the study and contributed to

744 writing the manuscript. HP and JK were involved in conducting the MiKlip historical simulations and writing the

745 manuscript

Competing interests

747 The authors do not declare any competing interests.

Acknowledgements

749 We like to thank the DKRZ for granting the computational resources during MiKlip.

Financial support

751 BMBF funded projects MiKlip-2 (Förderkennzeichen 01LP1517A and 01LP1519A) and SOLCHECK

752 (Förderkennzeichen 01LG1906C)

Review statement

754 We would like to thank Wenjuan Huo and the anonymous reviewer for taking the time to carefully review our

755 manuscript.

756

References

Allan, R., and Ansell, T.: A new globally complete monthly historical gridded mean sea level pressure dataset (HadSLP2): 1850–2004. J. Climate, 19(22), 5816-5842, doi.org/10.1175/JCLI3937.1, 2006.

Andrews, D. G.: Wave–mean-flow interaction in the middle atmosphere. In Adv. Geophys. (Vol. 28, pp. 249-275). Elsevier, doi.org/10.1016/S0065-2687(08)60226-5, 1985.

Andrews, M. B., Knight, J. R., and Gray, L. J.: A simulated lagged response of the North Atlantic Oscillation to the solar cycle over the period 1960–2009. Environ. Res. Lett., 10(5), 054022, doi10.1088/1748-9326/10/5/054022, 2015.

Arsenovic, P., Rozanov, E., Stenke, A., Funke, B., Wissing, J. M., Mursula, K., ... and Peter, T.: The influence of Middle Range Energy electrons on atmospheric chemistry and regional climate. J Atmos Sol Terr Phys., 149, 180-190, doi.org/10.1016/j.jastp.2016.04.008, 2016.

Baldwin, M. P., and Dunkerton, T. J.: Stratospheric harbingers of anomalous weather regimes. Science, 294(5542), 581-584. doi:10.1126/science.1063315, 2001.

Baumgaertner, A. J., Jöckel, P., Riede, H., Stiller, G., and Funke, B.: Energetic particle precipitation in ECHAM5/MESSy–Part 2: Solar proton events. Atmos. Chem. Phys., 10(15), 7285-7302, doi.org/10.5194/acp-10-7285-2010, 2010.

Bodeker, G. E., Boyd, I. S., and Matthews, W. A.: Trends and variability in vertical ozone and temperature profiles measured by ozonesondes at Lauder, New Zealand: 1986–1996. J. Geophys. Res., 103(D22), 28661-28681, doi.org/10.1029/98JD02581, 1998.

Butchart, N.: The Brewer-Dobson circulation. Rev. Geophys., 52(2), 157-184, https://doi.org/10.1002/2013RG000448, 2014.

Cagnazzo, C., Manzini, E., Giorgetta, M. A., Forster, P. M. D. F., and Morcrette, J. J.: Impact of an improved shortwave radiation scheme in the MAECHAM5 General Circulation Model, Atmos. Chem. Phys., 7, 2503–2515, https://doi.org/10.5194/acp-7-2503-2007, 2007.

Cionni, I., Eyring, V., Lamarque, J. F., Randel, W. J., Stevenson, D. S., Wu, F., ... and Waugh, D. W.: Ozone database in support of CMIP5 simulations: results and corresponding radiative forcing. Atmos. Chem. Phys., 11(21), 11267-11292, doi.org/10.5194/acp-11-11267-2011, 2011.

Chiodo, G., Calvo, N., Marsh, D. R., and Garcia-Herrera, R.: The 11year solar cycle signal in transient simulations from the Whole Atmosphere Community Climate Model. J. Geophys. Res., 117(D6), doi.org/10.1029/2011JD016393, 2012.

Chiodo, G., Oehrlein, J., Polvani, L. M., Fyfe, J. C., and Smith, A. K.: Insignificant influence of the 11-year solar cycle on the North Atlantic Oscillation. Nat. Geosci., 12(2), 94-99, doi.org/10.1038/s41561-018-0293-3, 2019.

Drews, A., Huo, W., Matthes, K., Kodera, K., and Kruschke, T.: The Sun's role in decadal climate predictability in the North Atlantic. Atmos. Chem. Phys., 22(12), 7893-7904, doi.org/10.5194/acp-22-7893-2022, 2022.

Eyring, V., Lamarque, J. F., Hess, P., Arfeuille, F., Bowman, K., Chipperfiel, M. P., ... and Young, P. Y.: Overview of IGAC/SPARC Chemistry-Climate Model Initiative (CCMI) community simulations in support of upcoming ozone and climate assessments. SPARC newsletter, 40 (Januar), 48-66, 2013.

Forster, P. M., et al.: Evaluation of radiation scheme performance within chemistry climate models, J. Geophys. Res., 116, D10302, doi:10.1029/2010JD015361, 2011.

Fouquart, Y., and Bonnel, B.: Computations of solar heating of the earth's atmosphere—A new parameterization, Beitr. Phy. Atmos., 53, 35–62, 1980.

Gray, L. J., et al.: Solar influences on climate, Rev. Geophys., 48, RG4001, doi:10.1029/2009RG000282, 2010.

Gray, L. J., Scaife, A. A., Mitchell, D. M., Osprey, S., Ineson, S., Hardiman, S., ... and Kodera, K.: A lagged response to the 11 year solar cycle in observed winter Atlantic/European weather patterns. J. Geophys. Res., 118(24), 13-405, doi.org/10.1002/2013JD020062, 2013.

Huang, J., Hitchcock, P., Maycock, A. C., McKenna, C. M., and Tian, W.: Northern hemisphere cold air outbreaks are more likely to be severe during weak polar vortex conditions. Communications Earth and Environment, 2(1), 147. doi.org/10.1038/s43247-021-00215-6, 2021.

805 Iacono, M. J., Delamere, J.S., Mlawer, E.J., Shephard, M. W., Clough, S. A., and Collins, W. D.: Radiative forcing

806   by long-lived greenhouse gases: Calculations with the AER radiative transfer models, J. Geophys. Res., 113,

807   D13103, doi:10.1029/2008JD009944, 2008.

808 Ilyina, T., Six, K. D., Segschneider, J., Maier-Reimer, E., Li, H., and Núñez-Riboni, I.: Global ocean

809   biogeochemistry model HAMOCC: Model architecture and performance as component of the MPI-Earth system

810   model in different CMIP5 experimental realizations. J. Adv. Model. Earth Syst., 5(2), 287-315,

811   doi.org/10.1029/2012MS000178, 2013.

812 Ineson, S., Scaife, A. A., Knight, J. R., Manners, J. C., Dunstone, N. J., Gray, L. J., and Haigh, J. D.: Solar forcing of

813   winter climate variability in the Northern Hemisphere. Nat. Geosci., 4(11), 753-757, doi.org/10.1038/ngeo1282,

814   2011.

815 Jackman, C. H., Marsh, D. R., Vitt, F. M., Garcia, R. R., Randall, C. E., Fleming, E. L. and Frith, S. M.: Long-term

816   middle atmospheric influence of very large solar proton events. J. Geophys. Res, 114(D11),

817   doi.org/10.1029/2008JD011415, 2009.

818 Jungclaus, J. H., Fischer, N., Haak, H., Lohmann, K., Marotzke, J., Matei, D., ... and Von Storch, J. S.:

819   Characteristics of the ocean simulations in the Max Planck Institute Ocean Model (MPIOM) the ocean

820   component of the MPI-Earth system model. J. Adv. Model. Earth Syst., 5(2), 422-446,

821   doi.org/10.1002/jame.20023, 2013.

822 Kodera, K.: Solar cycle modulation of the North Atlantic Oscillation: Implication in the spatial structure of the

823   NAO. Geophys. Res. Lett, 29(8), 59-1, doi.org/10.1029/2001GL014557, 2002.

824 Kodera, K., and Kuroda, Y.: Dynamical response to the solar cycle. J. Geophys. Res., 107(D24),

825   doi.org/10.1029/2002JD002224, ACL-5. 2002.

826 Kuroda, Y., Kodera, K., Yoshida, K., Yukimoto, S., & Gray, L.: Influence of the solar cycle on the North Atlantic

827   Oscillation. J. Geophys. Res., 127(1), e2021JD035519, doi.org/10.1029/2021JD035519, 2022.

828 Langematz, U., Kubin A., Brühl, C., Baumgaertner, A.J.G., Cubasch, U., and Spangehl, T.: Solar effects on

829   chemistry and climate including ocean interactions, in Climate And Weather of the Sun-Earth System

830   (CAWSES): Highlights from a Priority Program, F.-J. Lübken, ed., Springer, Dordrecht, The Netherlands, 2013.

Lean, J.: Evolution of the Sun's spectral irradiance since the Maunder Minimum. Geophys. Res. Lett., 27(16), 2425-2428, doi.org/10.1029/2000GL000043, 2000.

Ma, H., Chen, H., Gray, L., Zhou, L., Li, X., Wang, R. and Zhu, S.: Changing response of the North Atlantic/European winter climate to the 11-year solar cycle. Environ. Res. Lett., 13(3), 034007, doi10.1088/1748-9326/aa9e94, 2018.

Marotzke, J., Müller, W. A., Vamborg, F. S., Becker, P., Cubasch, U., Feldmann, H., ... and Ziese, M.: MiKlip: a national research project on decadal climate prediction. Bull. Am. Meteorol. Soc., 97(12), 2379-2394, https://doi.org/10.1175/BAMS-D-15-00184.1, 2016.

Matthes, K., Langematz, U., Gray, L. L., Kodera, K., and Labitzke, K.: Improved 11-year solar signal in the Freie Universität Berlin climate middle atmosphere model (FUB-CMAM). J. Geophys. Res., 109(D6), doi.org/10.1029/2003JD004012, 2004.

Matthes, K., Kuroda, Y., Kodera, K., and Langematz, U.: Transfer of the solar signal from the stratosphere to the troposphere: Northern winter. J. Geophys. Res., 111(D6), doi.org/10.1029/2005JD006283, 2006.

Matthes, K., Funke, B., Andersson, M. E., Barnard, L., Beer, J., Charbonneau, P., Clilverd, M. A., Dudok de Wit, T., Haberreiter, M., Hendry, A., Jackman, C. H., Kretzschmar, M., Kruschke, T., Kunze, M., Langematz, U., Marsh, D. R., Maycock, A. C., Misios, S., Rodger, C. J., Scaife, A. A., Seppälä, A., Shangguan, M., Sinnhuber, M., Tourpali, K., Usoskin, I., van de Kamp, M., Verronen, P. T., and Versick, S.: Solar forcing for CMIP6 (v3.2), Geosci. Model Dev., 10, 2247–2302, doi.org/10.5194/gmd-10-2247-2017, 2017.

Meehl, G. A., J. M. Arblaster, G. Branstator, and H. van Loon: A Coupled Air–Sea Response Mechanism to Solar Forcing in the Pacific Region. J. Climate, 21, 2883–2897, https://doi.org/10.1175/2007JCLI1776.1, 2008.

Meehl, G. A., Goddard, L., Boer, G., Burgman, R., Branstator, G., Cassou, C., ... and Yeager, S.; Decadal climate prediction: an update from the trenches. Bull. Am. Meteorol. Soc., 95(2), 243-267, doi.org/10.1175/BAMS-D-12-00241.1, 2014.

Mehta, V., Meehl, G., Goddard, L., Knight, J., Kumar, A., Latif, M., ... and Stammer, D.: Decadal climate predictability and prediction: where are we?. Bull. Am. Meteorol. Soc., 92(5), 637-640, doi.org/10.1175/2010BAMS3025.1, 2011.

hat gelöscht: Marsh, D. R., Garcia, R. R., Kinnison, D. E., Boville, B. A., Sassi, F., Solomon, S. C., and Matthes, K.: Modeling the whole atmosphere response to solar cycle changes in radiative and geomagnetic forcing. J. Geophys. Res., 112(D23), doi.org/10.1029/2006JD008306, 2007.¶

862 Misios, S. and Schmidt, H.: Mechanisms Involved in the Amplification of the 11-yr solar cycle signal in the tropical
863   Pacific Ocean, J. Climate, 25, 5102–5118, doi.org/10.1175/JCLID-11-00261.1, 2012.

864 Müller, W. A., Jungclaus, J. H., Mauritsen, T., Baehr, J., Bittner, M., Budich, R., ... and Marotzke, J: A higher-
865   resolution version of the max planck institute earth system model (MPI-ESM1. 2-HR). J. Adv. Model. Earth
866   Syst., 10(7), 1383-1413, doi.org/10.1029/2017MS001217, 2018.

867 Paulsen, H., Ilyina, T., Six, K. D., and Stemmler, I.: Incorporating a prognostic representation of marine nitrogen
868   fixers into the global ocean biogeochemical model HAMOCC. J. Adv. Model. Earth Syst., 9(1), 438-464,
869   doi.org/10.1002/2016MS000737, 2017.

870 Pohlmann, H., Müller, W. A., Kulkarni, K., Kameswarrao, M., Matei, D., Vamborg, F. S. E., Kadow, C., Illing, S.,
871   and Marotzke, J.: Improved forecast skill in the tropics in the new MiKlip decadal climate predictions, Geophys.
872   Res. Lett., 40, 5798– 5802, doi.10.1002/2013GL058051, 2013.

873 Pohlmann, H., Müller, W. A., Bittner, M., Hettrich, S., Modali, K., Pankatz, K., and Marotzke, J.: Realistic quasi-
874   biennial oscillation variability in historical and decadal hindcast simulations using CMIP6 forcing. Geophys.
875   Res. Lett., 46(23), 14118-14125, doi.org/10.1029/2019GL084878, 2019.

876 Randel, W. J., Smith, A. K., Wu, F., Zou, C., and Qian, H.: Stratospheric Temperature Trends over 1979–2015
877   Derived from Combined SSU, MLS, and SABER Satellite Observations, J. Climate, 29(13), 4843-4859,
878   doi.org/10.1175/JCLI-D-15-0629.1, 2016.

879 Reick, C. H., Raddatz, T., Brovkin, V., and Gayler, V.: Representation of natural and anthropogenic land cover
880   change in MPI-ESM. J. Adv. Model. Earth Syst., 5(3), 459-482, doi.org/10.1002/jame.20022, 2013.

881 Scaife, A. A., Ineson, S., Knight, J. R., Gray, L., Kodera, K., and Smith, D. M.: A mechanism for lagged North
882   Atlantic climate response to solar variability. Geophys. Res. Lett., 40(2), 434-439, doi.org/10.1002/grl.50099,
883   2013.

884 Scaife, A. A. and Smith, D.: A signal-to-noise paradox in climate science. NPJ Climate and Atmospheric Science,
885   1(1), 28, doi:10.1038/s41612-018-0038-4, 2018.

886 Seppälä, A., Randall, C. E., Clilverd, M. A., Rozanov, E., & Rodger, C. J.: Geomagnetic activity and polar surface
887   air temperature variability. J. Geophys. Res, 114(A10), doi.org/10.1029/2008JA014029, 2009.

888 Seppälä, A., Matthes, K., Randall, C. E. and Mironova, I. A.: What is the solar influence on climate? Overview of

889   activities during CAWSES-II. Progress in Earth and Planetary Science, 1(1), 1-12, doi.org/10.1186/s40645-014-

890   0024-3, 2014.

891 Schmidt, H., Brasseur, G. P., and Giorgetta, M. A.: Solar cycle signal in a general circulation and chemistry model

892   with internally generated quasi-biennial oscillation. J. Geophys. Res.,115(D1), doi.org/10.1029/2009JD012542,

893   2010.

894 Spiegl, T. and Langematz, U.: Twenty-First-Century Climate Change Hot Spots in the Light of a Weakening Sun.

895   Journal of Climate, 33(9), 3431-3447, doi.org/10.1175/JCLI-D-19-0059.1, 2020.

896 Stevens, B., et al.: Atmospheric component of the MPI-M Earth System Model: ECHAM6, J. Adv. Model. Earth

897   Syst., 5, 146–172, doi:10.1002/jame.20015, 2013.

898 Taylor, K. E., Stouffer, R. J., and Meehl, G. A.: An overview of CMIP5 and the experiment design. Bull. Am.

899   Meteorol. Soc., 93(4), 485-498. doi.org/10.1175/BAMS-D-11-00094.1, 2012.

900 Thiéblemont, R., Matthes, K., Omrani, N. E., Kodera, K., and Hansen, F.: Solar forcing synchronizes decadal North

901   Atlantic climate variability. Nat. Commun., 6(1), 8268, doi:10.1038/ncomms9268, 2015.

902

903